Microwave Photonic Systems for Demodulation of Optical Fiber Interference Signals

Yuru CHEN, Xiaohua LEI*, Xianming LIU, and Peng ZHANG

Key Lab of Optoelectronic Technology & Systems (Chongqing University), Ministry of Education, College of Optoelectronic Engineering, Chongqing University, Chongqing, 400044, China

*Corresponding author: Xiaohua LEI E-mail: xhlei@cqu.edu.cn

Abstract: Fiber optic sensors have been gradually used in aerospace, petrochemical, electronic power, civil engineering, and biomedical fields because of their many advantages such as the anti-electromagnetic interference, corrosion resistance, light weight, small size, high accuracy, and easy reuse. In recent years, sensing and demodulation technologies based on microwave photonics have attracted widespread attention. Optical fiber sensing combined with microwave photonics has higher sensitivity and flexibility, which is important for the demodulation of interferometric signals. This article introduces and analyzes the principle, structure, and performance of the demodulation technology of fiber optic interferometric signals based on microwave photonics from the perspective of system structures, such as filters, oscillators, and interferometers, and discusses the future research and development directions.

Keywords: Microwave photonics; optic fiber sensing; interference structure

Citation: Yuru CHEN, Xiaohua LEI, Xianming LIU, and Peng ZHANG, "Microwave Photonic Systems for Demodulation of Optical Fiber Interference Signals," *Photonic Sensors*, 2025, 15(1): 250122.

1. Introduction

With the emergence and evolution of low-loss optical fibers, as well as the development of fiber optic communication technologies and related fiber optic devices, the optic fiber sensing technology has been widely studied since the 1970s. The optic fiber sensing technology is based on the measurement of optical quantities and has the advantages of anti-electromagnetic interference, high sensitivity, simple structures, small sizes, compatibility with fiber optic structures, and the ability to transmit the sensing signal over long distances. It can be widely used in aerospace, petrochemical, electrical and electronic, civil engineering, and biomedical fields, as well as in the field of intelligent structure monitoring, such as monitoring the health status of buildings. Therefore, the study of fiber optic sensing has the great theoretical significance and engineering value.

The main technology of optic fiber sensing is to extract the information to be measured from the change of optical quantities, and the measurement of optical quantities becomes a key technology in optical fiber sensing because there are many different types of optical quantities to be measured in optical fiber sensing. From the classification of measurement signals, optic fiber sensing includes interferometric signals, fiber Bragg gating (FBG) reflectance spectra, scattering spectra, time domain pulse signals, and frequency domain pulse signals. Among them, the principle of the interferometric

Received: 11 July 2023 / Revised: 7 October 2023

DOI: 10.1007/s13320-024-0702-8
Article type: Review

signal is simple, the sensor structure is diverse and widely used, and the demodulation system is flexible and versatile. By exploring the demodulation method of the sensor, it is shown that efficient, accurate and fast demodulation methods are a key part to advance the practicability of optic fiber sensing.

In recent years, with the development of the microwave photonics (MWP) technology, it has shown significant advantages in high-frequency electrical signal generation and high-frequency electrical information processing, which can overcome the inherent bottleneck caused by the limited sampling speed in traditional electrical signal processors and has a wide range of applications [1–11]. Inspired by the development of the MWP technology, researchers in optical fiber sensing technologies hope to apply the MWP technology to fiber optic sensing to extract the information to be measured by demodulating the interferometric signal in the optical domain. The MWP technology converts the optical domain sensing information to the microwave domain, and the demodulation accuracy and demodulation rate can be improved. The cost of the demodulation equipment can be effectively reduced.

This article introduces and analyzes the principle, structure, and performance of the demodulation technology of fiber optic interferometric signals based on the microwave photons theory from the perspective of system structures, such as filters, oscillators, and interferometers, and discusses the future research and development directions.

2. Microwave photonic filter (MPF)

The MPF is one of the most important photonic signal processing techniques for broadband microwave signals. The functions of standard microwave filters used in telecommunication systems and radar radio frequency (RF) systems can be enhanced by the MPF, thus providing a greater range of tunability, reconfigurability, and a series of advantages, such as the immunity to electromagnetic interference. In this section, the principle of the MPF is briefly described, and then the parameters and characteristics of each system are analyzed from different types of the optical fiber interferometers.

2.1 General model for MPF

The classical MPF system is shown in Fig. 1. The basic structure of the MPF is similar to the microwave photonic link, which is composed of five basic components, such as the light source, interferometer, electro-optical modulator (EOM), photodetector (PD), and vector network analyzer (VNA). The light source can be a broadband light source, single frequency laser, and laser array. The interferometer mainly includes the Fabry-Perot interferometer (FPI), Mach-Zehnder interferometer (MZI), Michelson interferometer (MI), FBG, and fiber loop. The microwave signal is loaded onto the interferometric signal by the external modulation of the EOM. After completing the conversion from the electrical signal to optical signal, the optical signal is transmitted to the dispersion element for time delays, which is several kilometers of the single-mode fiber, dispersion-compensated fiber or chirped FBG. The PD then convert the optical signal back to the electrical signal. The measurement information carried by the interferometric signal can be demodulated by the VNA. The MPF takes full advantage of the low transmission loss and immunity to electromagnetic interference of optical fibers. Since the loss of modulation of RF signals at different frequencies through optical fibers is flat, the MPF is simpler to achieve the large range tunable and reconfigurable than other RF systems at high frequency bands.

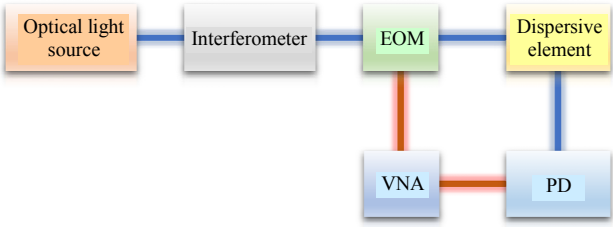

Fig. 1 Schematic diagram of the classic MPF system.

Let the spectral distribution of the light source be $S(\omega)$ and ω be the angular frequency of the light. The transfer function of the interferometer is $T(\omega)$. The interference signal generated by the interferometer is shown in Fig. 2, whose free spectral range (FSR) can be expressed as

$$\Delta\omega=\frac{2\pi c}{\mathrm{OPD}} \tag{1}$$

where OPD is the optical path difference (OPD) between interfering lights and c is the light speed.

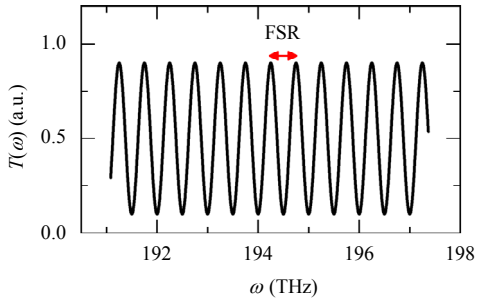

Fig. 2 Interference signal.

The interfering signal is modulated by the microwave with an angular frequency of Ω at the EOM. Taking the dispersion compensated fiber (DCF) as an example, the dispersive element can be considered as a phase filter with the mode equaling to (1), and its transmission function can be written as

$$H(\omega)=\left|H(\omega)\right|\mathrm{e}^{\mathrm{j}\Phi(\omega)}=\mathrm{e}^{\mathrm{j}\Phi(\omega)} \tag{2}$$

where the Taylor expansion of the phase term at ω_0 is [12]

$$\Phi(\omega)=\Phi(\omega_0)+\tau(\omega_0)(\omega-\omega_0)+\frac{1}{2}\beta L_{\mathrm{DCF}}(\omega-\omega_0)^2+\frac{1}{3}\chi L_{\mathrm{DCF}}(\omega-\omega_0)^3 \tag{3}$$

where $\tau(\omega_0)$ is the group delay at the frequency $\omega_0=2\pi c/\lambda_0$, and β, χ, and L_{DCF} are the dispersion coefficient, dispersion slope, and length of the dispersion compensated fiber, respectively.

After the optical signal passes through the interferometer, EOM and DCF, the microwave signal is finally collected at the PD as shown in Fig. 3. Then the frequency response of the system is given by [12]

$$H_{\mathrm{MPF}}(\Omega)=\int\left\{S(\omega)T(\omega)\left[H^*(\omega)H(\omega+\Omega)+H(\omega)H^*(\omega-\Omega)\right]\right\}\mathrm{d}\omega. \tag{4}$$

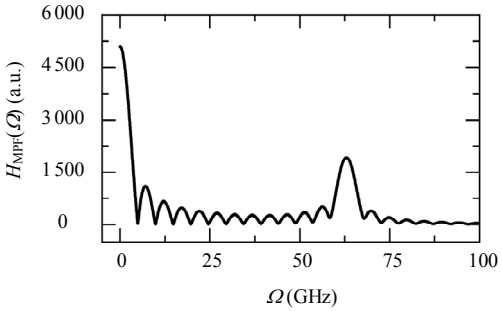

Fig. 3 Frequency response of the MPF system.

This frequency response is a single passband filter with the Gaussian distribution, whose passband central frequency can be expressed as

$$\Omega=\frac{2\pi}{\beta L_{\mathrm{DCF}}\Delta\omega}=\frac{1}{c\beta L_{\mathrm{DCF}}}\mathrm{OPD}. \tag{5}$$

From (5), it can be seen that the passband central frequency is related to the dispersion coefficient β and the FSR of the interferometric signal. Changing the physical parameter to be measured, such as the temperature, stress, or pressure, can change the FSR of the interferometric signal, thus causing the variation of the system frequency response of the MPF. Therefore, the physical quantity to be measured can be demodulated from the variation of the central frequency Ω. Moreover, the sensitivity of the traditional fiber optical interferometer is related to the OPD. According to (5), the sensitivity of the MPF is determined by the central frequency Ω, which is increased by a factor of $1/(\beta L_{\mathrm{DCF}})$. The combination of the MPF and the optical fiber sensing offers the advantage of high sensitivity.

Traditional optical fiber interferometers primarily include the structures like MZI, FPI, and MI. When there is an OPD between two optical signals, interference occurs, and the interference frequency is related to this OPD. The FPI is shown in Fig. 4(a). When the light transfer in the fiber from the left to right, the light is reflected by the two end faces of the FPI. The OPD equals to the double

length of the FP cavity length, which is 2L. The MZI is depicted in Fig. 4(b). The light is split into two paths by a coupler, and then join again at the second coupler. The OPD of the MZI is L_1–L_2. The MI is shown in Fig. 4(c). The light is split into two paths by a coupler getting the reflected back into the fiber by mirrors. The OPD of the MI is also L_1–L_2. As long as there is an OPD, interference can occur. Other special structures, such as FBG pairs and loops, can also be considered as the special interferometer, when there is an OPD.

The FPI, due to its small size and reflective structure, is commonly used for the measurement of the strain, pressure, and vibration. The MZI, with its long sensing arm, can enhance the sensing sensitivity and is suitable for measuring temperatures and transversal loads. The MI, with one arm serving as a reference arm and the other as a sensing arm, can be used for distance or gap measurement. Different interferometers have distinct advantages. Combining them with the MWP can offer even greater benefits.

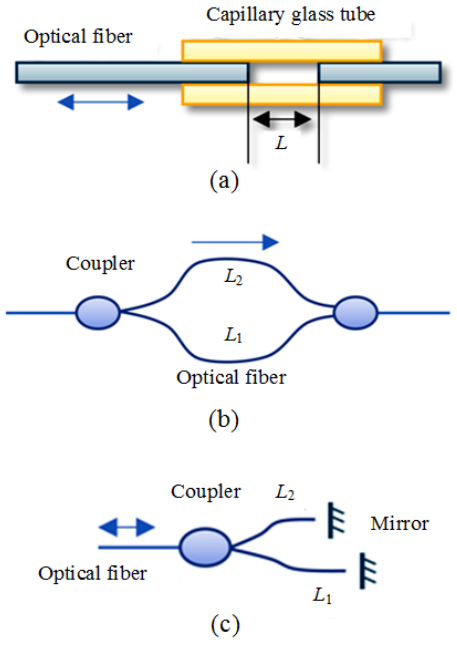

Fig. 4 Optical fiber interferometer: (a) FPI, (b) MZI, and (c) MI (all the optical fibers are the same in diameter, and the micro-structure of the FPI makes the optical fiber seem wider in diameter).

In this section, the statistics of MPF systems with different interferometers are presented. The light sources, interferometer types, sensing parameters, and sensitivity are shown in Table 1. The MPF systems are classified by the interferometer types in the following subsections.

Table 1 Statistics of MPF systems with different interferometers.

Ref.	Key interferometer	Light source	Parameter	Sensitivity
[13]	MZI	Broadband optical source (BOS)	Temperature	41.2 MHz/℃
[14]	MZI	BOS	Humidity	84 MHz/RH%
[15]	MZI	BOS	Temperature Transversal loading	0.077 dBm/℃, –13.76 MHz/℃ –0.0115 dBm/g, 0.147 MHz/g
[16]	MZI	Amplified spontaneous emission (ASE)	Curvature	–147.634 MHz/m^{-1}
[17]	MZI	ASE	Temperature	(33.55±4.17) MHz/℃
[18]	MZI	BOS	Temperature Transversal loading	8.51 MHz/℃, 16.85 MHz/℃ 17.1 dBm/N·m
[19]	FP	Broadband source (BBS)	Displacement	1 905.2 kHz/μm
[20, 21]	FP	ASE	Pressure	86 MHz/MPa
[22]	FBG-FP	BBS	Temperature	7×10^{-4}/℃ 11×10^{-4}/℃
[23]	MI	Optical amplifier	OPD	5.56 GHz/mm

2.2 MPF system based on the MZI

The most common interferometer used in the MPF is MZI. The interference signal is generated by the OPD between the two arms of the MZI, so the OPD is related to the passband central frequency of the MPF.

Taking the simplest MPF system as an example, the passband central frequency of the MPF can be changed by adjusting the OPD between the two arms of the MZI. Thus, the parameters of the MPF can vary with the application requirements [24–27]. As shown in Fig. 5 [24], the MZI interferometric frequency corresponds to the single passband frequency of the MPF system. One arm of the MZI has an optically variable delay line which allows the FSR of the interferometric signal to be adjusted.

Changes in the FSR allow the passband frequency to be shifted. Thus, the optically variable delay line allows the passband frequency of the MPF to be adjusted at will. This MPF offers high tuning linearity.

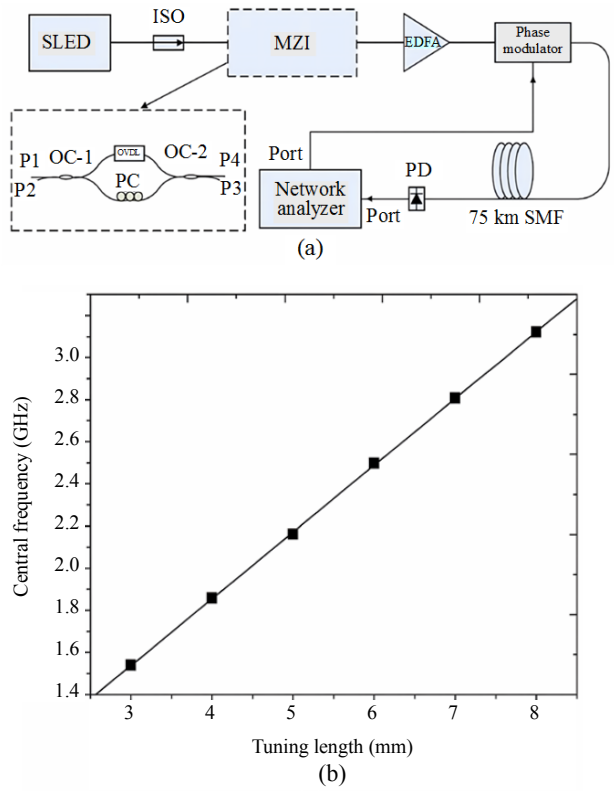

Fig. 5 MPF system based on the MZI: (a) experimental setup of the MPF based on the MZI (OVDL: optical variable delay line; SLED: superluminescent light-emitting diode; ISO: isolator; EDFA: erbium-doped fiber amplifier; SMF: single mode fiber; PC: polarization controller; OC: optical coupler; P: port) and (b) the relationship between the passband central frequency and the tuning length of the OVDL (solid rectangular: measured results; solid line: linearly fitted line) [24].

This linear relationship between the OPD in the MZI and the passband central frequency can be applied to measure various physical quantities, such as temperatures, transversal loads, and humidity [13–15]. As shown in Fig. 6 [14], a section of the POF is fused to one arm of the MZI to measure the humidity of the environment. The humidity drives a change in the FSR of the MZI interferometric signal, which shifts the passband frequency of the MPF. This system has the humidity sensitivity of 84 MHz/RH% and resolution of 0.0119 RH%. The advantages of high resolution and resistance to vibration enable it to be used in harsh environments.

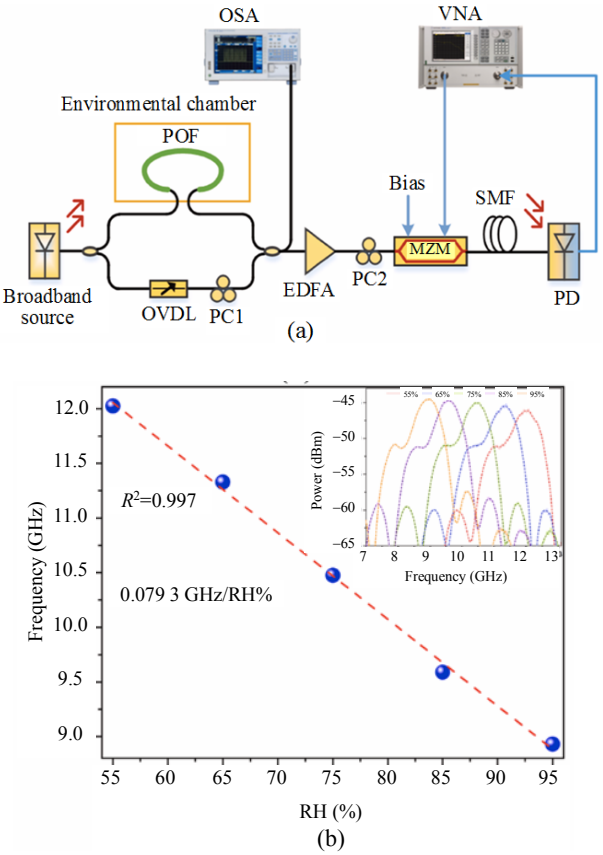

Fig. 6 MPF humidity sensing system based on the MZI: (a) experimental setup of the proposed humidity sensor (POF: polymer optical fiber; MZM: Mach-Zehnder modulator; OSA: optical spectrum analyzer) and (b) measured frequency shift of the microwave photonic filter's passband with different relative humidity (RH) settings when the OVDL is tuned (inset: the corresponding frequency responses) [14].

In addition to the single arm of the MZI, which can measure physics, the two arms can also be used separately for multi-parameters measurement. As shown in Figs. 7 and 8 [15], one arm of the MZI is used to measure the temperature and the other arm is used to measure the transversal loading. The transversal loading has an effect on the polarization state of the light, while the temperature has an effect on the refractive index of the fiber. Both are related to the central frequency and amplitude of the passband of the MPF. Measuring the central frequency and amplitude gives information on the temperature and loading. The sensitivity of this

system to changes in temperatures and transversal loadings (including cross coefficients) is 0.147 MHz/g, 0.077 dBm/℃, –13.76 MHz/℃, and –0.0115 dBm/g, respectively.

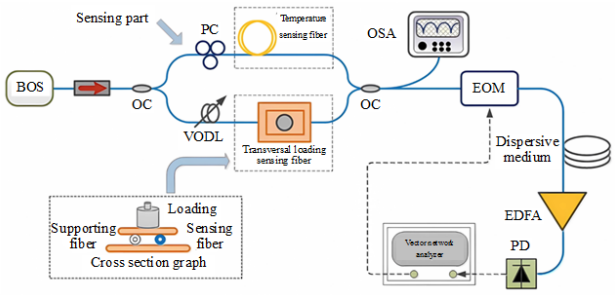

Fig. 7 Schematic diagram of the proposed fiber-optic sensing interrogation system for simultaneous measurement of temperatures and transversal loadings (BOS: broadband optical source; EOM: electrical-optical modulator) [15].

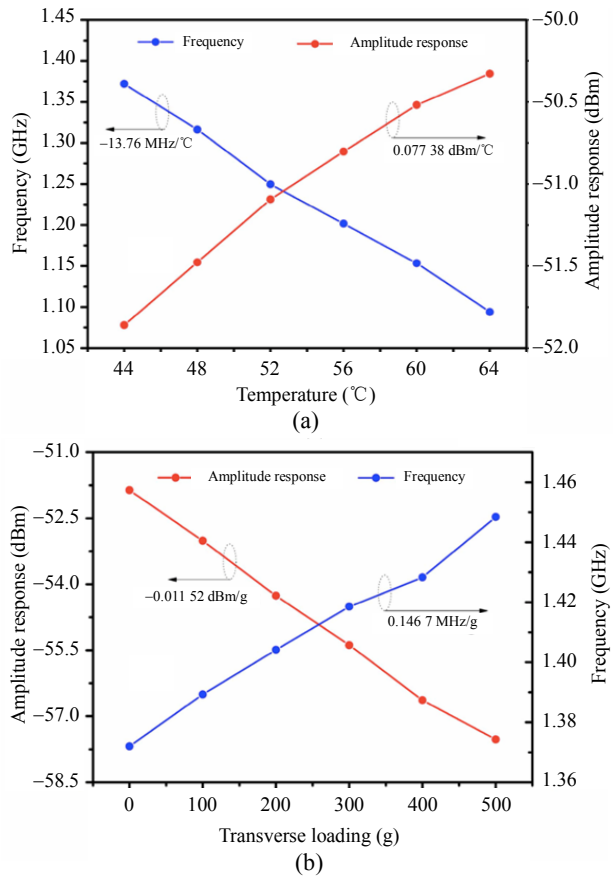

Fig. 8 Measured response of peak frequency: (a) amplitude to the temperature and (b) transversal loading [15].

More research has been carried out on the analysis and improvement of MZI structures, the ability to measure multiple parameters independently, and the formation of multi-passband filters [16–18, 28–30]. As shown in Fig. 9 [30], the infrastructure of this system is the same as that of the MZI-based MPF system described above. The innovation is the upgrade of the MZI, as shown in Fig. 10(a) [30]. The cascade and reflection structure allows the MZI to have multiple interferometric frequencies which correspond to the central frequencies of the MPF passbands. The system therefore has multiple passbands in its frequency response function, as shown in Fig. 10(b). A system with multiple passbands is able to measure more physical parameters. Thus, it owns the advantages of the simple principle, clear structure, and high flexibility.

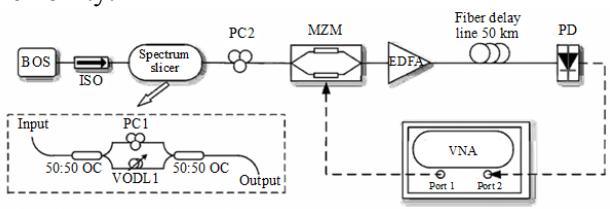

Fig. 9 Schematic diagram of the proposed MPF and the structure of the optical slicer based on a fiber MZI (FMZI) (VODL: variable optical delay line) [30].

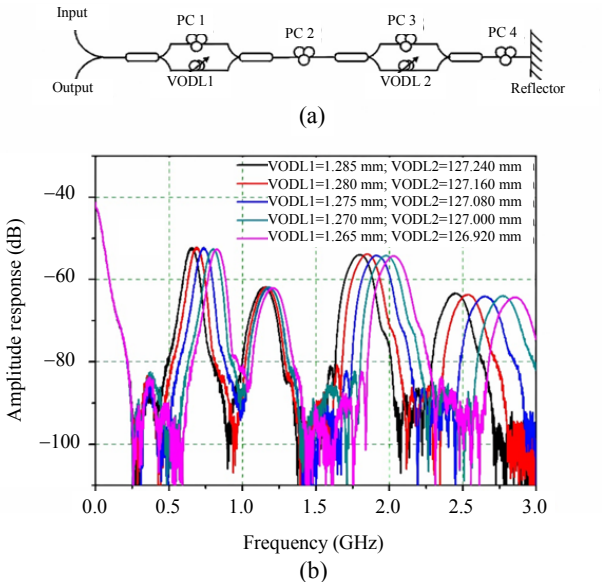

Fig. 10 MPF system based on the cascaded MZIs: (a) schematic diagram of the reflective cascaded FMZIs and (b) measured frequency responses to the variation of different VODLs [30].

2.3 MPF system based on the FPI

For some physical parameters, such as pressure and clearance, the FPI is required. As with the MZI, the interferometric frequency of the FPI corresponds to the passband central frequency of the MPF [19–21, 31]. As shown in Fig. 11(a) [20], the broadband light source, external FPI (EFPI), phase modulator (PM), and DCF make up the pressure single passband MPF system. The pressure is related to the interferometric FSR of the EFPI and thus to the offset of the passband central frequency of the MPF. The EFPI-based microwave photonic system has high-pressure resolution than the conventional fiber optic sensing systems based on spectral analysis. The sensitivity of the sensor was measured in the range of 0 MPa–4 MPa up to 86 MHz/MPa, as shown in Fig. 11(b).

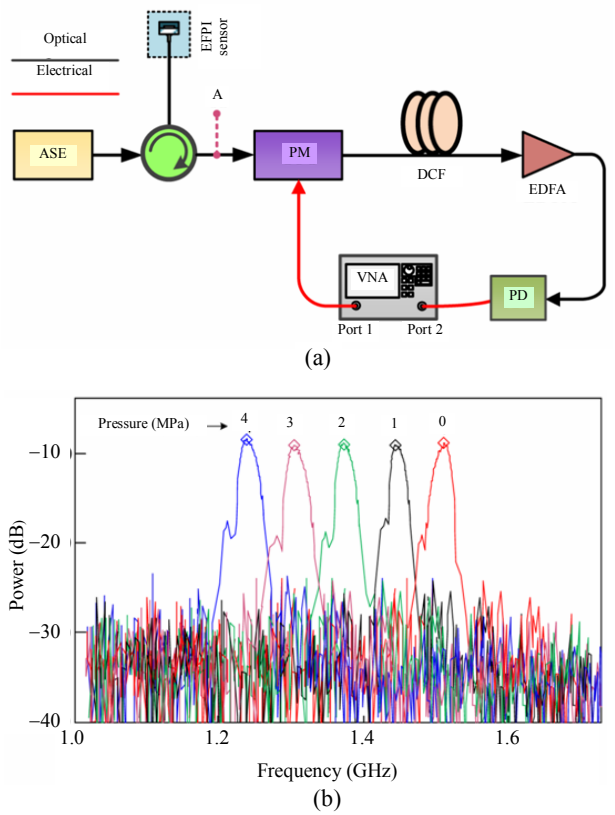

Fig. 11 MPF system based on the FPI: (a) schematic of the proposed pressure sensing system and (b) measured frequency responses of the MPF when different pressure is applied [20].

2.4 MPF system based on the FBG

FBG structures are highly flexible in the optical fiber sensing technology and can generate interferometric signals from two FBGs or an array of FBGs [22, 32–34]. As shown in Fig. 12 [22], two FBGs form an FBG-FP sensing head, and an interferometric signal is generated between the FBGs, corresponding to an MPF passband central frequency. Two FBG-FP sensing heads correspond to two MPF central frequencies. When the temperature change is applied to the sensing heads, the passband central frequencies are shifted, as shown in Fig. 13. The ratio of the central frequency shifts between the two sensing heads contributes to the sensitivity of the response and reduces the effects of crosstalk.

2.5 Others

In addition to the interferometers, such as MZI, FPI, and FBG-FP, there are also interferometers such as the fiber loops as well as MI that can generate interference signals [23, 35]. All of these interferometers can be used to modulate the passband central frequency of the MPF by adjusting the OPD. As shown in Fig. 14, two mirror-reflective optical paths form the MI, which generates the interference signal. Due to the high optical losses in microwave photonic systems, the mirror-reflective structure facilitates the increase of optical power in the system. The MI can be used for displacement measurement. There is a highly linear relationship between the OPD in the MI and the passband central frequency. The displacement sensitivity is 5.56 GHz/mm, and the displacement resolution is 124 μm.

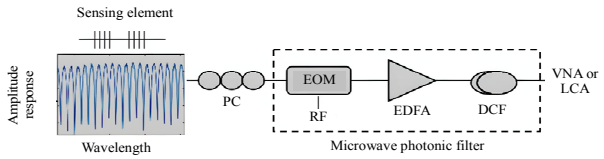

Fig. 12 MWP-based sensor interrogation system (LCA: lightwave component analyzer) [22].

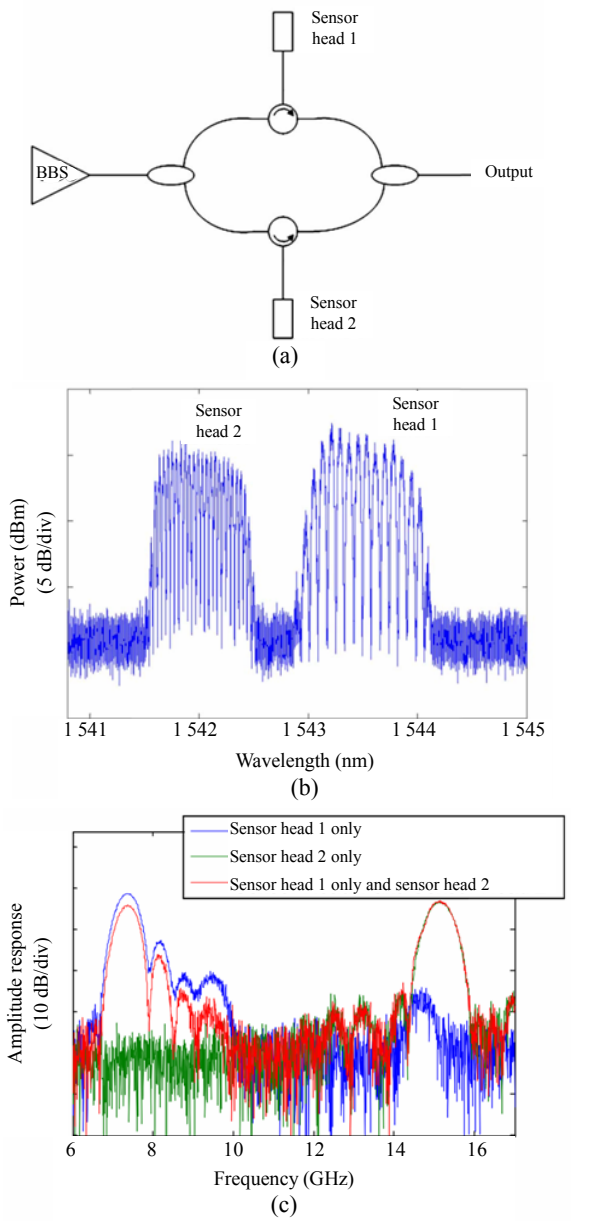

Fig. 13 MPF system based on two FBG-FPI sensors: (a) experimental setup implementing the input to the MPF system used to achieve dual-temperature sensing: Sensor heads 1 and 2 correspond to FBG-FPs 1 and 2, respectively, (b) spectrum of the multi-wavelength input source to the MPF and (c) MPF responses [22].

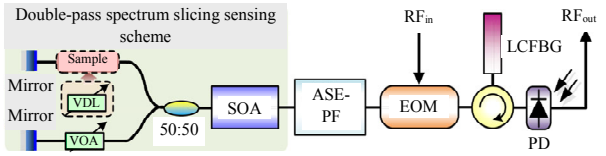

Fig. 14 Schematic diagram of the microwave photonic sensing system using a reflective double-pass sensing-source-based configuration (VOA: variable optical attenuation; SOA: semiconductor optical amplifier; ASE-PF: amplified spontaneous emission-profiler filter; LCFBG: linearly chirped fiber Bragg grating.) [23].

3. Microwave photonic filter and optoelectronic oscillator

The previous section is an exposition and analysis of MPF systems based on different types of interferometers. This section is an introduction to microwave photonic systems combining the MPF and optoelectronic oscillator (OEO) [36–41]. In contrast to the MPF system, the MPF+OEO system has both the frequency response of the single-pass band of the MPF and the characteristics of the oscillating signal generated by the OEO. An oscillator is a device that transfers energy from a light source to a periodically varying signal and is an important device used in a wide range of industries. Oscillators include a wide range of mechanical oscillators, electromagnetic ones, and atomic ones, all of which have the potential for achieving the ideal harmonic oscillator. The performance of an oscillator can be measured by the spectral purity and stability of the output signal, which is determined by the loss of the various devices in the loop, depending on the oscillator's ability to store energy. The OEO is an excellent optoelectronic hybrid resonant loop that produces signal stability comparable to that produced by the best crystal oscillators.

The MPF+OEO system is shown in Fig. 15. The hardware difference between it and the MPF system is that there is no more VNA that is the RF source and analyzer. The electrical microwave signal of the PD is amplified by the electrical amplifier (EA) and fed back into the electro-optical modulator (OEM). This system has no microwave input signals. The OEO structure performs periodic frequency selection by means of the oscillatory feedback of the system noise and converts the energy of the optical light source into the selected microwave frequencies. The single passband of the MPF acts as a filter, which is able to filter out again the desired frequencies from the periodic frequencies selected by the OEO.

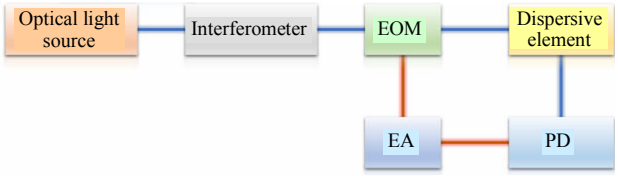

Fig. 15 MPF+OEO microwave photonic system.

The transfer function for OEO is [42]

$$P(\Omega)=\frac{\dfrac{G_A^2\left|\widetilde{V}(\Omega)\right|^2}{2R}}{\left\{\begin{array}{l}1+\left|F(\Omega)G(V_0)\right|^2-\\ 2F(\Omega)\left|G(V_0)\right|\cos\left[\Omega\tau'+\phi(\Omega)+\phi_0\right]\end{array}\right\}} \quad (6)$$

where G_A is the gain factor of the electrical amplifier, $G(\cdot)$ is the open-loop voltage gain factor, R is the impedance of the PD, $\widetilde{V}$ is the complex form of the output voltage, V_0 is the amplitude of the input electrical signal, $F(\cdot)$ is the system frequency dependent function, Ω is the microwave angular frequency, τ' is the loop delay, ϕ is the phase, and ϕ_0 is the phase bias of the modulator.

The frequency response of the OEO is a series of periodic frequencies, whose frequencies are determined by the following equation:

$$\Omega\tau'+\phi(\Omega)+\phi_0=2k\pi,\quad k=0,\,1,\,2,\cdots. \quad (7)$$

The frequency response of the MPF+OEO system is determined by both (5) and (7). Only the OEO oscillation frequency within the single passband of the MPF will respond, as shown in Fig. 16.

The MPF+OEO microwave photonic system combines the advantages of the high sensitivity of the MPF system and the good signal stability of the OEO system. The different interferometer types allow this system to be used in different measurement environments, as shown in Table 2.

Table 2 Statistics of MPF+OEO systems with different interferometers.

Ref.	Key interferometer	Light source	Parameter	Sensitivity
[37]	MZI	BOS	Cu^{2+} ions concentration	13 Hz/(μM/L)
[39]	MZI	ASE	Temperature	3.7 MHz/℃
[36]	MI	BOS	Temperature Strain	–16.4 MHz/℃ –0.29 MHz/με
[41]	Optical frequency comb	Diode laser	Strain	-

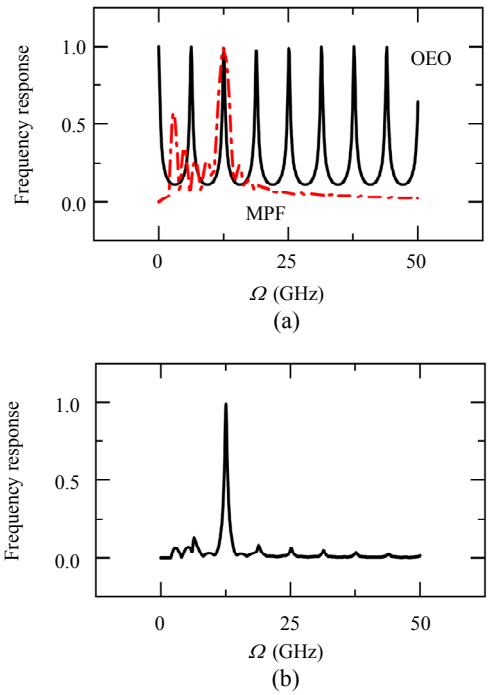

Fig. 16 Frequency response of the different systems: (a) frequency response of MPF and OEO systems and (b) frequency response of the MPF+OEO system.

As shown in Fig. 17 [39], the microwave photonic system of the MPF+OEO can be used to measure temperatures. The frequency response of the system is determined by both the passband central frequency of the MPF and the OEO oscillation frequency. One arm of the MZI is used as a reference arm and the other arm as a temperature sensor. The temperature affects the FSR of the MZI interferometric signal. The frequency of the system response is thus shifted. The role of the MPF is sensing and demodulation. And the function of the OEO is to generate the microwave signal. The temperature sensitivity of the whole system reaches 3.7 MHz/℃.

The OEO+MPF system based on the MI is shown in Fig. 18 [36]. The MI can be used to measure distances or clearance. The OEO system generates a high-quality microwave signal and the MPF system demodulates the parameters to be measured. Compared to the conventional MI optical fiber sensing systems, the MPF+OEO system

increases the sensing sensitivity. In addition, the wavelength-to-frequency mapping of the DCF and the broadband tunability of the OEO avoid the overlap of the MI periodic spectrum. This system also offers the advantage of large-scale sensing.

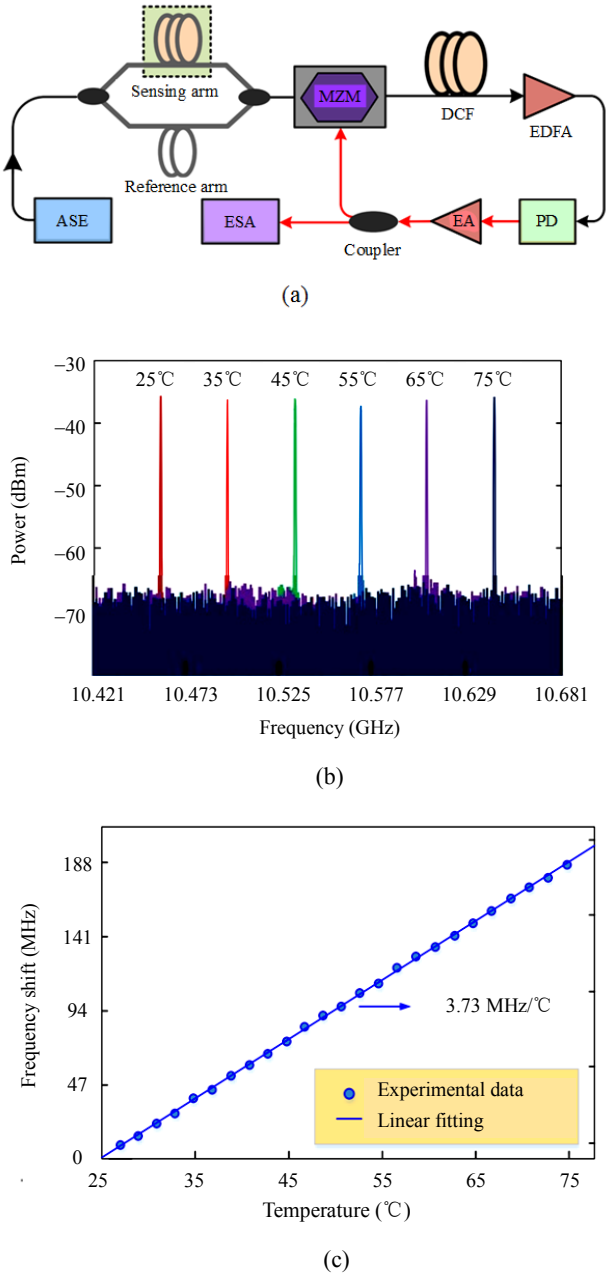

Fig. 17 MPF+OEO system: (a) schematic of the proposed OEO based sensing system (ESA: electrical spectrum analyzer), (b) superimposed electrical spectra of the generated microwave signal at different temperatures, and (c) measured oscillation frequency shift as the function of the applied temperature to the sensing arm from 25 ℃ to 75 ℃ with a step of 2 ℃ [39].

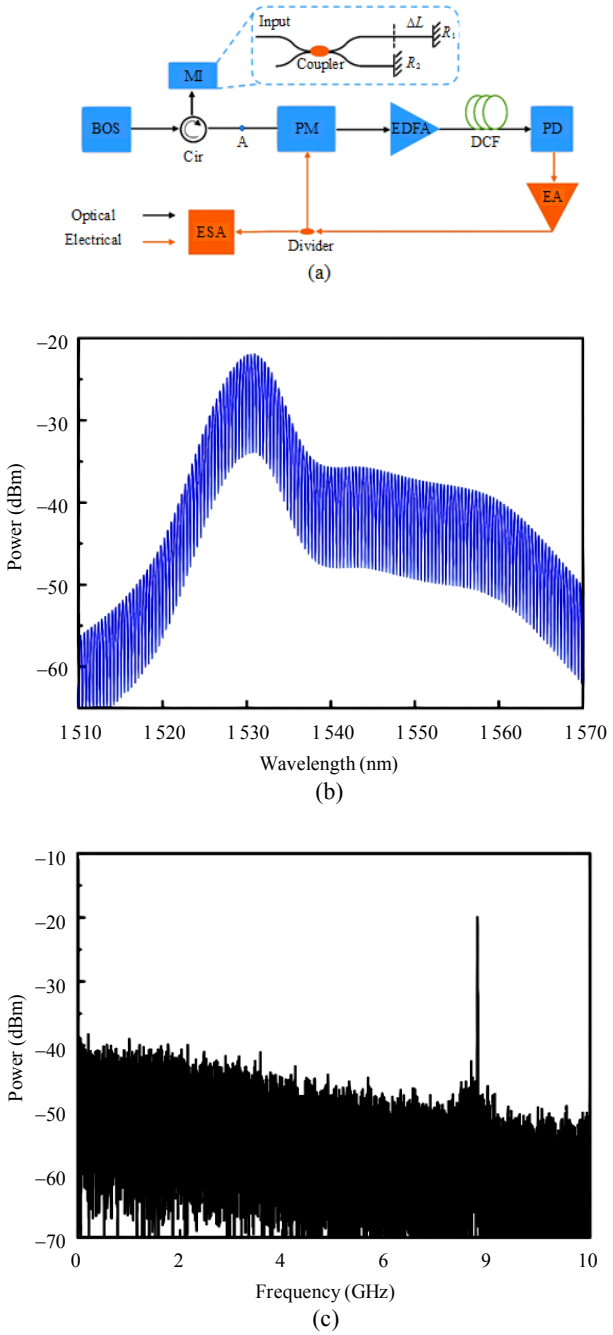

Fig. 18 MI+OEO system: (a) schematic of the proposed interrogation system, (b) optical spectrum of the sinusoidal broadband optical signal generated via the MI, and (c) electrical spectrum of the OEO-generated signal [36].

4. Microwave interferometer (MWI)

In the conventional optical fiber sensing systems, the sensitivity of the sensor and the corresponding resolution are usually limited by the light source used in the system as well as the spectral detection device (such as the OSA). In addition to this, the

conventional methods also make it difficult to demodulate and multiplex a large number of optical fibre sensors at the same time. In 2014, Clemson [43, 44] proposed a sensing system by microwave modulation of optical carriers to generate microwave interference. The main idea of the microwave interference system is to use the same electromagnetic properties of light waves and microwaves, and microwave fields are stronger and also more stable than light field signals, because the phase of the microwave envelop signals are thus stable enough for coherent superposition. The fiber optical interference is susceptible to the interference between the multi-modes of the multi-modes fiber or the sapphire fiber. The microwave interference is much stable in these fibers. So, the interference phenomena occurring in the optical field are transferred to the stable microwave field.

The difference between the MWI and MPF is that the interference in the MWI occurs in the microwave field, while that in the MPF occurs in the optical field.

4.1 General model for MWI

The schematic diagram of the MWI sensing system is shown in Fig. 19. A light signal from a light source is fed into a modulator and modulated by a microwave sweep frequency signal generated by the VNA, which can be controlled and adjusted according to requirements. The signal from the modulator is a modulated microwave signal, which is then transmitted into the interferometer, which can also be selected according to demands, such as the MI, MZI, and FPI. It is the interferometer where the microwave interference phenomenon occurs. And then the microwave interference signal is detected by a high-speed detector and sent back to the VNA for the corresponding calculation, analysis, and display, i.e., the microwave interference spectrum pattern with all the information of light waves can be plotted. When the environment changes, parameter sensing is achieved based on the change in microwave responses.

The microwave interference spectrum of an MWI sensing system can be expressed as [43]

$$I_{\mathrm{MWI}}(\Omega,t)=2A^2+\left\{\begin{array}{l}2A^2M\cos\left(\Omega\dfrac{L_1-L_2}{2c}\right)\times\\ \cos\left[\Omega\left(t+\dfrac{2W+L_1+L_2}{2c}\right)\right]\end{array}\right\}+2A^2\sqrt{\left\{1+M\cos\left[\Omega\left(t+\dfrac{W+L_1}{2c}\right)\right]\right\}\times\left\{1+M\cos\left[\Omega\left(t+\dfrac{W+L_2}{2c}\right)\right]\right\}}\times\int_{\omega_{\min}}^{\omega_{\max}}\cos\left(\omega\frac{L_1-L_2}{c}\right)\mathrm{d}\omega \quad (8)$$

where W is the same electrical length of the microwave path, L_1 and L_2 denote the optical paths of the two modulated signals, Ω is the microwave angular frequency, ω is the optical angular frequency, t is time, A is the electric field amplitude vector, and M is the modulation intensity.

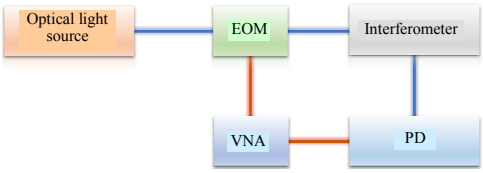

Fig. 19 Diagram of the MWI system.

Equation (8) shows three basic terms of this signal: the DC item, microwave interference item, and the light wave interference item. When the optical range difference OPD=L_1–L_2 is much larger than the coherence length of the light source, then the integral term in the third item can be approximated as zero, so the optical interference signal term is zero. The second item including all the information of the microwave signal is detected by a high-speed PD to ensure that its detection frequency is synchronized with the microwave frequency to achieve the synchronous detection, thus automatically excluding the value of the DC signal term. The microwave interference term in (1) can be obtained by scanning a range of microwave frequencies through the VNA. The microwave interference term contains the amplitude and phase

of the microwave interference signal. The phase information is a function of the total length between the VNA and the PD, which is the sum of the electrical and optical lengths. The amplitude information depends on the OPD. When the OPD changes, the microwave interference signal changes accordingly. This is the principle underlying MWI sensing.

In this section, the statistics of MPF systems with different interferometers are presented in Table 3. The MWI systems are classified by the interferometer types in the following subsections.

Table 3 Statistics of MWI systems with different interferometers.

Ref.	Key interferometer	Light source	Parameter	Sensitivity
[44]	MI	BBS	Temperature	−64 kHz/℃
[45]	MZI	Laser	Temperature	−6.1 kHz/℃
[46]	MZI	ASE	Strain	0.008 35 a.u./με
[47]	MZI	Laser	Transversal loading	15.625 MHz/N
[48]	MZI	BBS	Curvature	92 MHz/m^{-1}
[49]	MZI	Tunable laser source	Strain	103.94 KHz/με
[50]	MZI	ASE	Transversal loading	2.5 MHz/N
[51]	MZI	ASE	Curvature	0.425 μs/℃
[52]	Loop	BOS	Temperature	−556.856 kHz/℃
[53]	Loop	BOS	Temperature; Transversal Loading	25.73 kHz/℃; 204.92 dBm/N·m
[54]	Loop	Laser	Displacement	−71.28 ns/mm
[55]	Loop	BBS	Strain	-
[56]	FPI	BBS	Strain	0.002 4 nm/με
[57]	FPI	BBS	Distance	-
[58]	FBG-FPI	BBS	Strain	−0.34 μV/με
[59]	FBG-FPI	ASE	Strain	53.57 kHz/με
[60, 61]	Distributed FPI	BBS	Strain	−343.7 kHz/με
[62]	Distributed FPI	FP laser	Strain	-
[63]	Distributed FPI	Laser	Strain	-
[64]	Distributed FPI	BBS	Strain	−2.26 kHz/με
[65]	Distributed FPI	ASE	Strain	-
[66]	MI	ASE	Temperature; Strain	−2.647 kHz/με −15.54 kHz/℃

4.2 MWI system based on the MZI

The core of the MWI system is the interferometer. The MZI is one of the most versatile interferometers. The OPD between the arms of the MZI can directly affect the microwave interference frequency.

The most typical and simple application of the MZI considers one arm as a sensor [46, 48–50, 67–71]. As shown in Fig. 20 [45], this is a microwave interference system based on the MZI. Microwave interference occurs at the MZI when a microwave is loaded onto an optical signal, and the interferometric signal is acquired by the PD. The interference signal can be analyzed by the network analyzer (NWA) in the microwave domain. The NWA outputs microwaves at different frequencies, and the interferometric signal can be observed in this microwave frequency range. One arm of the MZI is treated as a temperature sensor. The temperature sensitivity is –6.1 kHz/℃ and the temperature resolution is 0.4 ℃.

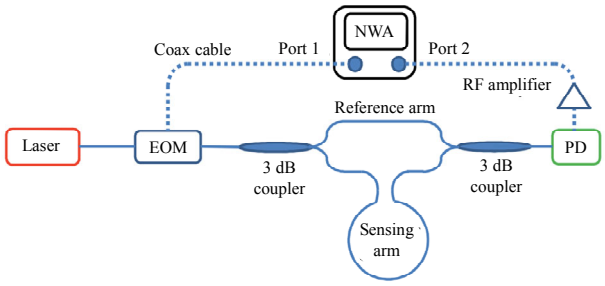

Fig. 20 Schematic of the RF-MZI sensor and instrumentation for interrogation (dotted lines are the coaxial cable and solid lines are the optical fiber link) [45].

There is also a lot of research on the flexibility of the MZI [47, 51, 72]. As shown in Fig. 21 [47], this is an MWI system using a polarization-maintaining photonic-crystal fiber (PM-PCF) as a transversal load sensor. The two different polarized lights have different degrees of the response to the transversal load. Their interference frequencies are linearly related to the load. The transversal load can be determined by the amount of notch frequency shift of the microwave interference signal. The system has the transverse load sensitivity of up to 15.625 MHz/N.

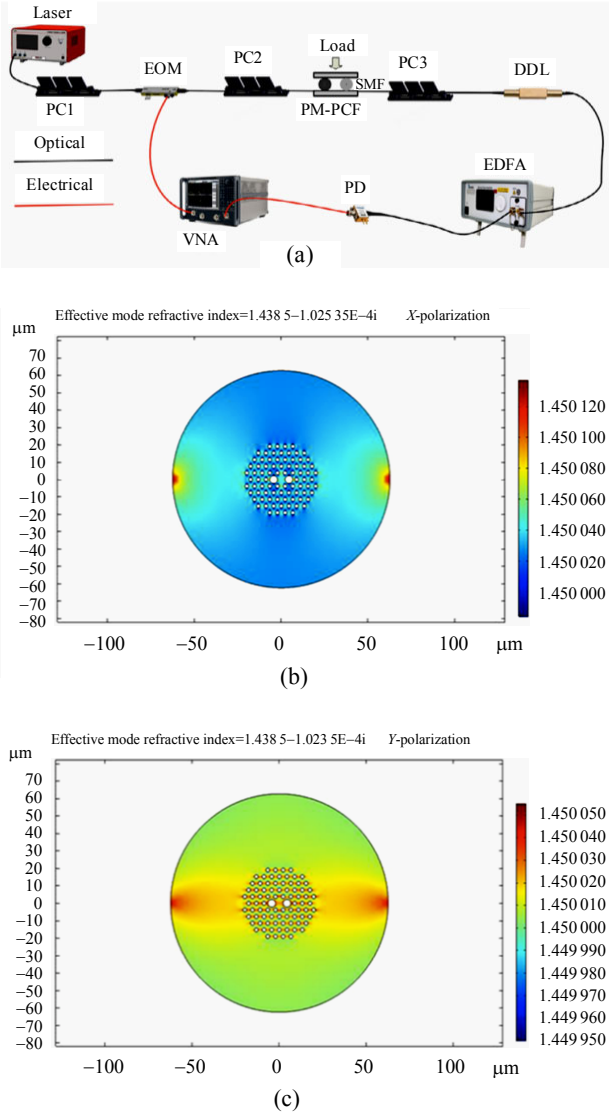

Fig. 21 Load sensing MI system based on the MZI: (a) schematic of the proposed microwave photonic sensing system (PM-PCF: polarization-maintaining photonic-crystal fiber; DDL: differential delay line); (b) and (c) the refractive index profiles along the *x* and *y* axes at the load of 4 N [47].

Combining MZI and the Loop enables the ability to measure temperatures and curvature separately. As shown in Fig. 22 [51], there is a fiber loop on each arm of the MZI and the fiber loops are used to sensing physical parameters. The MWI system does not require a high-quality light source, as the interference occurs in the microwave domain. The light source is just a carrier wave. This system is characterized by fast response time and high flexibility. The sensitivity of the system is 0.425 μs/℃ in the temperature range of 30 ℃–70 ℃ and 0.1553 μs/cm^{-1} in the curvature range of 0.8696 cm^{-1}–1.0526 cm^{-1}.

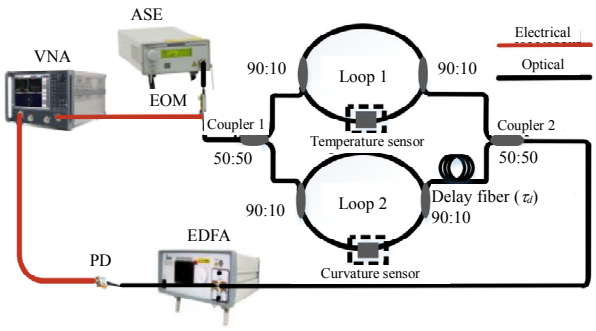

Fig. 22 Schematic diagram of the multi-function sensing system [51] (τ_d is the extra time delay induced by the delay fiber in Loop 2).

4.3 MWI system based on the loop

The fiber loop is a special structure, which can be seen as an infinitely repetitive sampling element with the equal time interval. The fiber loop is composed of the input and output of the coupler connected to achieve continuous sampling and time delays of the optical carrier microwave signal. The light wave enters the fiber ring again through the input of the coupler, repeats the same beam splitting and combining process infinitely, and experiences the equal time delay. The infinitely equal time interval optical signal arrives at the PD and generates an interference signal [52–55, 73–76]. As shown in Fig. 23(a) [53], this is a fiber loop MWI system that measures temperatures and transversal loadings. The temperature affects the interference frequency of the fiber loop. The transversal loading causes a change in the micro-bending loss, which affects the extinction ratio of the interference. The peak frequency and extinction ratio of the interference characterize the physical parameters of the temperature and transversal loading, respectively. This MWI system has the advantages of high sensitivity, tailorability, good linearity, and high multiplexing capability, and has great potential for applications.

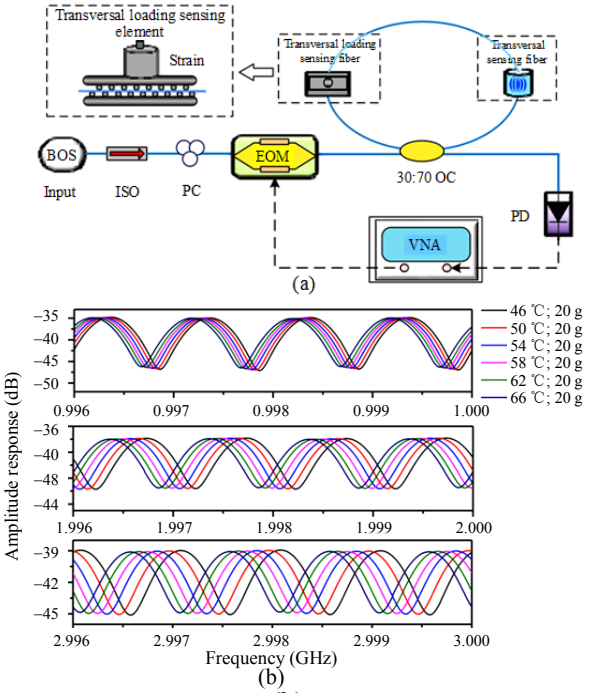

Fig. 23 MI system based on the loop: (a) schematic diagram of the proposed fiber-optic sensing system and (b) the frequency response around 1 GHz, 2 GHz, and 3 GHz of the proposed sensing system at different temperatures with 20 g transversal loading applied [53].

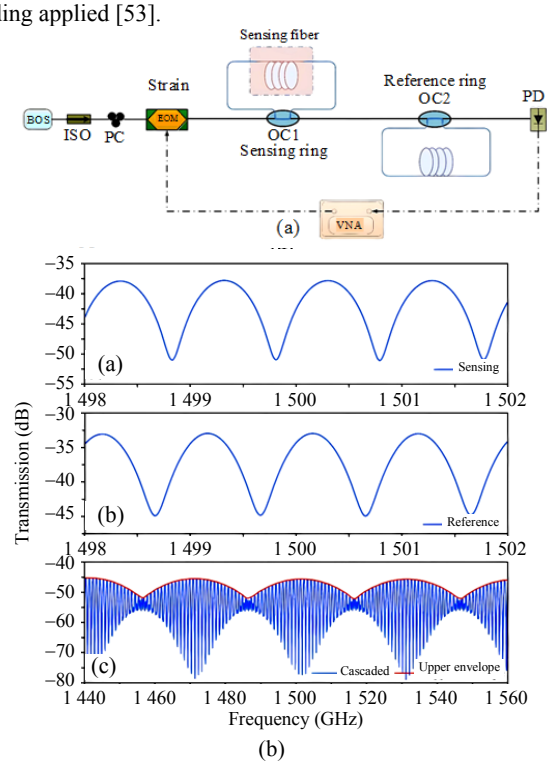

Fig. 24 MI system based on the cascaded loop: (a) schematic diagram of the cascaded fiber ring based on the sensor (OC: optical coupler) and (b) frequency response of the system with just the sensing fiber ring, just the reference ring, two cascaded fiber rings (red line: upper envelope of the frequency response curve) [52].

The fiber loop is applied in a variety of ways. As shown in Fig. 24(a) [52], this is an MWI system with cascaded fiber loops. One fiber loop is used as a temperature sensor and the other fiber loop is used as a reference. The frequency response curve of the MWI system is linear in the frequency shift and temperature. The cascaded fiber loops have a Vernier effect when the optical path of the two fiber loops is slightly different, as shown in Fig. 24(b). Compared to a single fiber loop, the cascaded fiber loops can increase the temperature sensitivity about 30 times.

4.4 MWI system based on the FPI and its distributed applications

The FPI has a very wide range of applications due to its properties of reflecting light from two end surfaces to produce interference signals [43, 56–59, 77]. The optical fiber FPI has been widely used for accurate measurement of various physical chemical quantities (e.g., the temperature, strain, pressure, rotation, and refractive index.). However, the random variation of the polarization state along the fiber direction and the strong dependence on the optical waveguide material and geometry are challenges for obtaining high-quality interferometric signals. Meanwhile, the difficulty of multiplexing has been a bottleneck for the FPI development. As shown in Fig. 25 [43], this MWI system has both the optical and microwave advantages, such as the resistance to electromagnetic interference and the insensitivity to optical waveguides. The microwave interference frequency is low, so the optical differences including the mode dispersion and polarization dispersion are not significant. Microwave interference occurs at the sensor head. The microwave interference frequency and phase information can resolve the physical quantity to be measured.

Unlike the conventional fiber optic sensing, the FPI is commonly used for distributed sensing in the

microwave domain [60–65, 78, 79]. As shown in Fig. 26 [64], it is an MWI system with spatially continuous distributed sensing. There are many FPIs with different optical paths in the MWI system, and the positions of these FPIs correspond to their microwave interference frequencies. This multiplexed FPIs can be used for distributed measurement of strain and other physics, chemistry, and biology parameters. The sensing sensitivity of strain is –2.26 KHz/με and the spatial resolution is 3 cm.

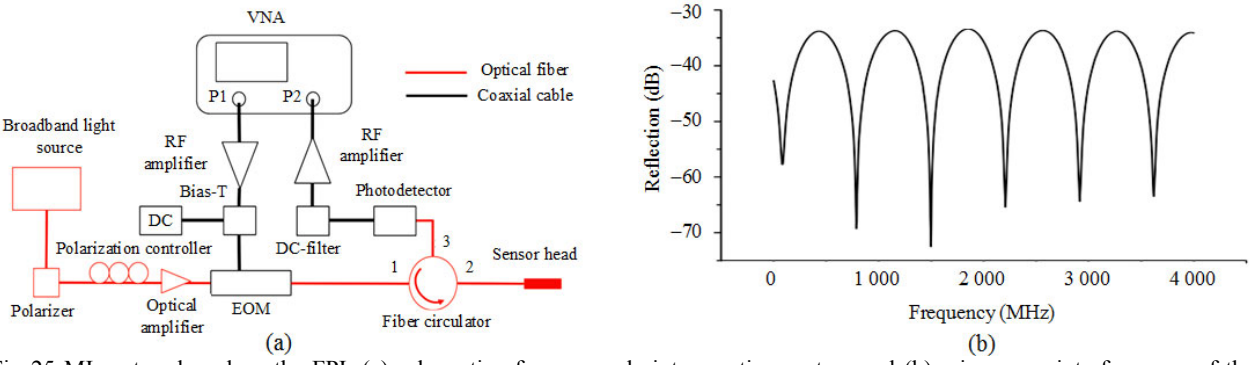

Fig. 25 MI system based on the FPI: (a) schematic of an example interrogation system and (b) microwave interferogram of the multi-modes fiber based on FPI [43].

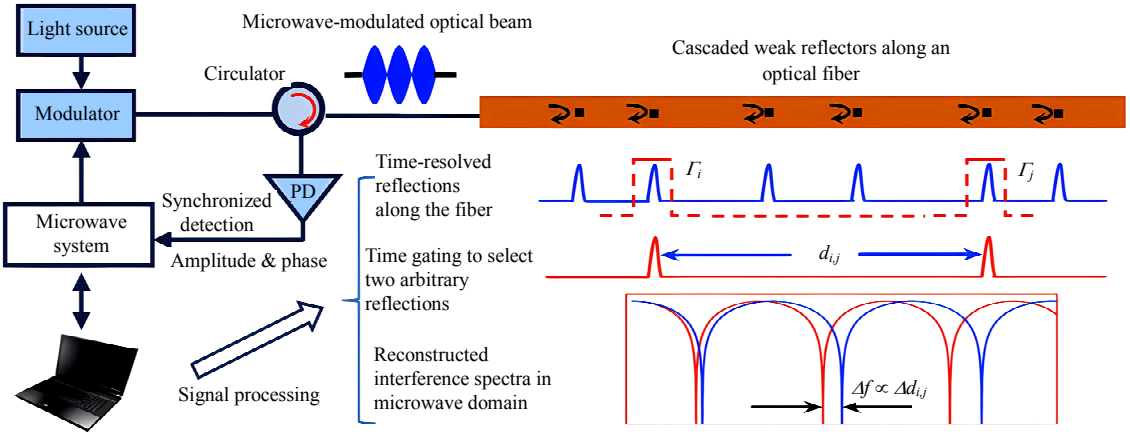

Fig. 26 Schematic illustration of the fundamental concept of the spatially continuous distributed sensing using cascaded FPIs. The segmentation is achieved by implementing a time-gating function with two windows to isolate two arbitrary reflections (e.g., *i* and *j*) for reconstruction of the microwave interference, whose spectral shift is proportional to the length change of the segment between the *i*th and *j*th reflectors (i.e., $d_{i,j}$) [64].

4.5 MWI system based on MI

The MWI systems based on the MI have unique advantages in measuring certain parameters, such as the temperature [44, 66, 80]. As shown in Fig. 27 [44], this is a sapphire MWI system for high-temperature sensing. A high-quality interference spectrum with the fringe visibility of over 40 dB occurs at the MI. Sapphire has high temperature resistance. The MI made of sapphire is used as a temperature sensor. This temperature sensor shows good sensitivity, reversibility, and stability in the temperature range of 100 ℃–1 400 ℃. There exists the problem of intermodal interference of sapphire and the effect of the background blackbody radiation light at a high temperature in the conventional optical fiber sensing systems. However, the microwave interference in MWI systems is insensitive to both multi-modes effects and blackbody radiation, offering unique advantages. The temperature sensitivity is –64 kHz/℃.

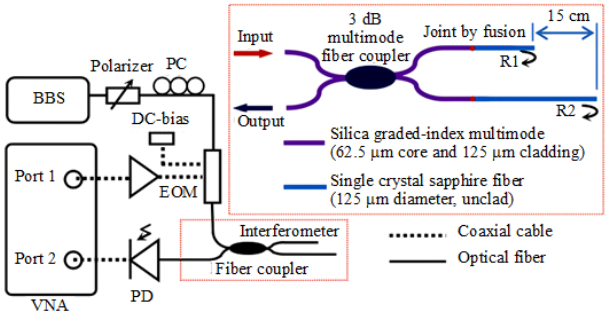

Fig. 27 Schematic of the interrogation system (MA: microwave amplifier; color inset: schematic of the sapphire based on the MI) [44].

5. Conclusions

Microwave photonic systems based on different types of interferometers combine the sensitivity of optical devices and the potential advantages of processing information in the microwave domain. Therefore, research on microwave photonic sensing methods has developed rapidly. However, there are still many problems to be solved for microwave photonic systems.

(1) System demodulation rate. For MPF and MWI systems, the most common microwave signal source is the VNA, which can also perform microwave spectrum analysis. But a complete microwave spectrum is related to the number of microwaves and output rate of the VNA. So, the demodulation rate of the system is limited by the VNA.

(2) Multi-parameter sensing. Most of microwave photonic systems are now capable of measuring two parameters at the same time. In some special occasions, sensing of multiple physical quantities is required. Therefore, the measurement of three or more physical quantities is still under research.

(3) Intermodal interference. There is intermodal interference in optical domain interference. The microwave interference in MWI systems can avoid intermodal interference. However, for MPF and MPF+OEO systems, some special fibers, such as the sapphire fiber, still have the problem of optical domain intermodal interference. These problems limit the further development of microwave photonic systems.

(4) Minimum interferometric length. There is the minimum interferometric length in microwaves. The interferometer of the MWI system does not have the problem of intermodal interference, but the OPD of the interference must be larger than the coherence length of the microwave. This requires the big size of the interferometer and cannot be applied to some fine spaces. So, this is also a restriction on the MWI system.

Acknowledgment

This work was supported in part by the National Natural Science Foundation of China (Grant Nos. 52175530, 51675068, 51975077, and 61875023).

Declarations

Conflict of Interest The authors declare that they have no competing interests.

Permissions All the included figures, tables, or text passages that have already been published elsewhere have obtained the permission from the copyright owner(s) for both the print and online format.

References

[1] X. Zou, B. Lu, W. Pan, L. Yan, A. Stöhr, and J. Yao, "Photonics for microwave measurements," *Laser and Photonics Reviews*, 2016, 10(5): 711–734.

[2] J. Capmany, B. Ortega, and D. Pastor, "A tutorial on microwave photonic filters," *Journal of Lightwave Technology*, 2006, 24(1): 201–229.

[3] Z. Zou, X. Liu, W. Li, P. Li, W. Pan, L. Yan, *et al.*, "Optoelectronic oscillators (OEOs) to sensing, measurement, and detection," *IEEE Journal of Quantum Electronics*, 2016, 52(1): 1–16.

[4] H. Fu, D. Chen, and Z. Cai, "Fiber sensor systems based on fiber laser and microwave photonic technologies," *Sensors*, 2012, 12(1): 5395–5419.

[5] X. Yi, S. Chew, S. Song, L. Nguyen, and R.

Minasian, "Integrated microwave photonics for wideband signal processing," *Photonics*, 2017, 4(46): 1–14.

[6] L. Li, X. Yi, S. Song, S. Chew, R. Minasian, and L. Nguyen, "Microwave photonic signal processing and sensing based on optical filtering," *Applied Sciences*, 2019, 9(163): 1–12.

[7] J. Hervas, A. Ricchiuti, W. Li, N. Zhu, C. Fernandez-pousa, S. Sales, *et al.*, "Microwave photonics for optical sensors," *IEEE Journal of Selected Topics in Quantum Electronics*, 2017, 23(2): 1–13.

[8] J. Yao, "Optoelectronic oscillators for high speed and high resolution optical sensing," *Journal of Lightwave Technology*, 2017, 35(16): 3489–3497.

[9] S. Iezekiel, "Integrated microwave photonics: a key enabling technology for radio-over-fiber," *Broadband Access Communication Technologies XI*, 2017, 1012803: 10–17.

[10] J. Yao, "Microwave photonic systems," *Journal of Lightwave Technology*, 2022, 40(20): 6595–6607.

[11] J. Yao, "Microwave photonics," *Science China-Information Sciences*, 2022, 65(1): 221401.

[12] J. Mora, B. Ortega, A. Diez, J. L. Cruz, M. V. Andres, J. Capmany, *et al.*, "Photonic microwave tunable single-bandpass filter based on a Mach-Zehnder interferometer," *Journal of Lightwave Technology*, 2006, 24(7): 2500–2509.

[13] H. Chen, S. Zhang, H. Fu, B. Zhou, and N. Chen, "Sensing interrogation technique for fiber-optic interferometer type of sensors based on a single-passband RF filter," *Optics Express*, 2016, 24(1): 255797.

[14] X. Cheng, J. Hu, K. Zhu, and Z. Zhao, "High-resolution polymer optical fibre humidity sensor utilizing single-passband microwave photonic filter," *Measurement*, 2021, 179(1): 109462.

[15] S. Zhang, R. Wu, H. Chen, H. Fu, J. Li, L. Zhang, *et al.*, "Fiber-optic sensing interrogation system for simultaneous measurement of temperature and transversal loading based on a single-passband RF filter," *IEEE Sensors Journal*, 2017, 17(7): 2036–2041.

[16] D. Xiao, G. Wang, F. Yu, S. Liu, W. Xu, L. Shao, *et al.*, "Optical curvature sensor with high resolution based on in-line fiber Mach-Zehnder interferometer and microwave photonic filter," *Optics Express*, 2022, 30(4): 5402–5413.

[17] X. Tian, Y. Wang, J. Shi, L. Gao, and D. Zhu, "Improving the sensitivity of temperature measurement based on a dual-passband microwave photonic filter," *IEEE Sensors Journal*, 2022, 22(21): 20531–20537.

[18] X. Chen, H. Chen, R. Wu, H. Fu, and X. Wang, "Simultaneous measurement of temperature and transversal loading by using a modified fiber Mach-Zehnder interferometer," *IEEE Sensors Journal*, 2018, 18(1): 2776–2781.

[19] C. Fernandez-paousa, H. Maestre, and P. Corral, "Interferometric displacement sensor by use of a single-passband incoherent microwave photonics filter," in *23rd International Conference on Optical Fibre Sensors*, Santander, 2014, pp. 1482–1485.

[20] Y. Wang, X. Ni, M. Wang, Y. Cui, and Q. Shi, "Demodulation of an optical fiber MEMS pressure sensor based on single bandpass microwave photonic filter," *Optics Express*, 2017, 25(2): 644–653.

[21] Y. Wang, M. Wang, X. Ni, W. Xia, D. Guo, H. Hao, *et al.*, "An optical fiber MEMS pressure sensor using microwave photonics filtering technique," in *Proc. 25th International Conference on Optical Fiber Sensors*, Jeju, 2017, pp. 1032368.

[22] M. Comanici, L. Chen, and P. Kung, "Microwave photonic filter-based interrogation system for multiple fiber Bragg grating sensors," *Applied Optics*, 2017, 56(32): 9074–9078.

[23] L. Li, X. Yi, S. Chew, S. Song, L. Nguyen, and R. Minasian, "Double-pass microwave photonic sensing system based on low-coherence interferometry," *Optics Letters*, 2019, 44(7): 1662–1665.

[24] H. Fu, K. Zhu, H. Ou, and S. He, "A tunable single-passband microwave photonic filter with positive and negative taps using a fiber Mach-Zehnder interferometer and phase modulation," *Optics and Laser Technology*, 2010, 42(1): 81–84.

[25] Z. Zhang, Y. Zhang, L. Zhang, Y. Xu, Y. He, S. Zhang, *et al.*, "Frequency response measurement of Mach-Zehnder modulators utilizing double carrier based on low frequency detection," in *Proc. Real-time Photonic Measurements, Data Management, and Processing VI*, Nantong, Jiangsu, 2021, pp. 1190211.

[26] J. Mora, B. Ortega, A. Diez, J. Cruz, M. Andres, J. Capmany, *et al.*, "A single bandpass tunable photonic transversal filter based on a broadband optical source and a Mach-Zehnder interferometer," in *International Topical Meeting on Microwave Photonics*, Budapest, 2003, pp. 251–254.

[27] L. Li, X. Yi, T. Huang, and B. Minasian, "Shifted dispersion-induced radio-frequency fading in microwave photonic filters using a dual-input Mach–Zehnder electro-optic modulator," *Optics Letters*, 2013, 38(7): 1164–1166.

[28] Z. Xu, H. Fu, H. Chen, C. Wu, H. Xu, and Z. Cai, "Microwave photonic filter with two independently

tunable passbands based on paralleled fiber Mach–Zehnder interferometers and dispersive medium," *Applied Physics B–Lasers and Optics*, 2015, 120(3): 557–562.

[29] R. Wu, H. Chen, S. Zhang, and H. Fu, "A switchable and tunable dual-passband microwave photonic filter," in *Progress in Electromagnetic Research Symposium. IEEE*, Shanghai, 2016, pp. 1588–1591.

[30] R. Wu, H. Chen, S. Zhang, H. Fu, Z. Luo, L. Zhang, *et al.*, "A tunable and selectable multi-passband microwave photonic filter utilizing reflective and cascaded fiber Mach-Zehnder interferometers," *Journal of Lightwave Technology*, 2016, 35(13): 2660–2668.

[31] J. Benitez, M. Bolea, and J. Mora, "Demonstration of multiplexed sensor system combining low coherence interferometry and microwave photonics," *Optics Express*, 2017, 25(11): 12182–12187.

[32] B. Gwandu, W. Zhang, J. Williams, L. Zhang, and I. Bennion, "Microwave photonic filtering using Gaussian-profiled superstructured fibre Bragg grating and dispersive fibre," *Electronics Letters*, 2002, 38(22): 1328–1330.

[33] J. Capmany, J. Mora, B. Ortega, and D. Pastor, "High-Q microwave photonic filter with a tuned modulator," *Optics Letters*, 2005, 30(17): 2299–2301.

[34] J. Mora, M. Andres, J. Cruz, B. Ortega, J. Capmany, D. Pastor, *et al.*, "Unable all-optical negative multitap microwave filters based on uniform fiber Bragg gratings," *Optics Letters*, 2003, 28(15): 1308–1310.

[35] J. Mora, L. Chen, and J. Capmany, "Single-bandpass microwave photonic filter with tuning and reconfiguration capabilities," *Journal of Lightwave Technology*, 2008, 26(15): 2663–2670.

[36] L. Liu, T. Ning, X. Sun, J. Xu, J. Zhang, and H. You, "Sensing interrogation system with Michelson interferometer incorporating an optoelectronic oscillator," in *Advanced Sensor Systems and Applications XI*, Jiangsu, 2021, pp. 119010P.

[37] D. Ming, X. Liu, D. Feng, Y. Tang, and T. Zhu, "Trace copper detection using in-line optical fiber Mach-Zehnder interferometer combined with an optoelectronic oscillator," *Optics Express*, 2021, 29(15): 23430–23438.

[38] D. Feng, Y. Gao, T. Zhu, M. Deng, X. Zhang, and L. Kai, "High-precision temperature-compensated magnetic field sensor based on optoelectronic oscillator," *Journal of Lightwave Technology*, 2021, 39(8): 2559–2564.

[39] Y. Wang, J. Zhang, and J. Yao, "An optoelectronic oscillator for high sensitivity temperature sensing," *IEEE Photonics Technology Letters*, 2016, 28(13): 1458–1461.

[40] X. Xue, X. Zheng, H. Zhang, and B. Zhou, "Widely tunable single-bandpass microwave photonic filter employing a non-sliced broadband optical source," *Optics Express*, 2011, 19(19): 18423–18429.

[41] G. Gagliardi, M. Salza, S. Avino, P. Ferraro, and P. Natale, "Probing the ultimate limit of fiber-optic strain sensing," *Science*, 2010, 330(6007): 1081–1084.

[42] T. Hao, Y. Liu, J. Tang, Q. Cen, W. Li, N. Zhu, *et al.*, "Recent advances in optoelectronic oscillators," *Advanced Photonics*, 2020, 2(04): 4–23.

[43] J. Huang, X. Lan, H. Wang, L. Yuan, and H. Xiao, "Optical carrier-based microwave interferometers for sensing application," in *Fiber Optic Sensors and Applications XI*, Baltimore, United States, 2014, pp. 90980H.

[44] J. Huang, W. Lan, Y. Song, Y. Li, W. Hua, and H. Xiao, "Microwave interrogated sapphire fiber Michelson interferometer for high temperature sensing," *IEEE Photonics Technology Letters*, 2015, 27(13): 1398–1401.

[45] T. Wei, J. Huang, X. Lan, Q. Han, and H. Xiao, "Optical fiber sensor based on a radio frequency Mach-Zehnder interferometer," *Optics Letters*, 2012, 37(4): 647–649.

[46] J. Zhou, L. Xia, R. Cheng, Y. Wen, and J. Rohollahnejad, "Radio-frequency unbalanced M-Z interferometer for wavelength interrogation of fiber Bragg grating sensors," *Optics Letters*, 2016, 41(2): 313–316.

[47] Z. Song, Y. Wang, and Y. Cheng, "Demodulation of a polarization-maintaining photonic crystal fiber load sensor with high resolution using a microwave photonic filter," *Microwave and Optical Technology Letters*, 2020, 63(6): 1612–1615.

[48] D. Zheng, J. Madrigal, D. Barrera, S. Sales, and J. Capmany, "Microwave photonic filtering for interrogating FBG-based multicore fiber curvature sensor," *IEEE Photonics Technology Letters*, 2017, 29;(20;): 1707–1710.

[49] Y. She, Y. Wang, J. Shi, X. Tian, and D. Zhu, "Novel interrogation method for fully distributed LCFBG sensor based on microwave photonic filtering," *IEEE Photonics Technology Letters*, 2022, 34(23): 1304–1307.

[50] Y. Wang, M. Wang, W. Xia, and X. Ni, "High-resolution fiber Bragg grating based transverse load sensor using microwave photonics filtering technique," *Optics Express*, 2016, 24(16): 17960–17967.

[51] X. Wu, Y. Wang, J. Shi, and D. Zhu, "A microwave photonic-assisted fiber loop ring down system with multi-sensing function," *IEEE Photonics Technology Letters*, 2022, 34(2): 117–120.

[52] Z. Xu, X. Shu, and H. Fu, "Sensitivity enhanced fiber sensor based on a fiber ring microwave photonic filter with the Vernier effect," *Optics Express*, 2017, 25(18): 21559–21566.

[53] S. Li, R. Wu, H. Wang, X. Chen, P. Fu, H. Fu, *et al.*, "Fiber-ring-based RF filtering for temperature and transversal loading measurement and interrogation," *IEEE Sensors Journal*, 2018, 18(14): 5794–5798.

[54] C. Zhu, Y. Zhuang, and J. Huang, "Sensitivity-enhanced fiber-optic sensor in a microwave photonics fiber loop ringdown system," *Journal of Lightwave Technology*, 2022, 40(16): 5768–5774.

[55] H. Fu, W. Zhang, C. Mou, X. Shu, L. Zhang, S. He, *et al.*, "High-frequency fiber Bragg grating sensing interrogation system using Sagnac-loop-based microwave photonic filtering," *IEEE Photonics Technology Letters*, 2009, 21(8): 519–521.

[56] L. Hua, "Microwave assisted reconstruction of optical interferograms for distributed optics sensing & characterization of PCB dielectric properties using two striplines on the same board," Ph.D. dissertation, Missouri University, Columbia, MO, 2014.

[57] Z. Hou, J. Kang, J. Yue, H. Li, T. Xue, and B. Wu, "Method of high-precision spatial distance measurement based on optical-carried microwave interference," *Optics Express*, 2022, 30(11): 18762–18771.

[58] X. Dong, L. Shao, H. Fu, H. Tam, and C. Lu, "Intensity-modulated fiber Bragg grating sensor system based on radio-frequency signal measurement," *Optics Letters*, 2008, 33(5): 482–484.

[59] R. Cheng, L. Xia, J. Yan, J. Zhou, Y. Wen, and J. Rohollahnejad, "Radio frequency FBG-based interferometer for remote adaptive strain monitoring," *IEEE Photonics Technology Letters*, 2015, 27(15): 1577–1580.

[60] C. Zhu and J. Huang, "High-sensitivity optical fiber sensing based on a computational and distributed Vernier effect," *Optics Express*, 2022, 30(21): 37566–37578.

[61] C. Zhu, M. Roman, Y. Zhuang, and J. Huang, "Distributed fiber optic sensing with enhanced sensitivity based on microwave-photonic Vernier effect," *Optics Letters*, 2022, 47(11): 2810–2813.

[62] X. Zhu, L. Hua, J. Lei, J. Tang, L. Murdoch, and H. Xiao, "Microwave-photonic low-coherence interferometry for dark zone free distributed optical fiber sensing," *Optics Letters*, 2021, 46(5): 1173–1176.

[63] L. Hua, Y. Song, B. Cheng, W. Zhu, Q. Zhang, and H. Xiao, "Coherence-length-gated distributed optical fiber sensing based on microwave-photonic interferometry," *Optics Express*, 2017, 25(11): 31362–31376.

[64] J. Huang, X. Lan, M. Luo, and H. Xiao, "Spatially continuous distributed fiber optic sensing using optical carrier based microwave interferometry," *Optics Express*, 2014, 22(15): 18757–18769.

[65] L. Hua, Y. Song, J. Huang, B. Cheng, W. Zhu, and H. Xiao, "Femtosecond laser fabricated multimode fiber sensors interrogated by optical-carrier-based microwave interferometry technique for distributed strain sensing," in *Photonic Instrumentation Engineering III*, San Francisco, 2016, pp. 91540V.

[66] L. Hua, Y. Song, J. Huang, W. Lan, Y. Li, and H. Xiao, "Microwave interrogated large core fused silica fiber Michelson interferometer for strain sensing," *Applied Optics*, 2015, 54(24): 7181–7187.

[67] C. Zhu, J. Wang, and J. Huang, "Group delay manipulation in a passive microwave-photonic fiber optic Mach–Zehnder interferometer," *Optics Letters*, 2022, 47(18): 4688–4691.

[68] J. Zhang, X. Luo, J. Wo, X. Li, A. Wang, J. Zhang, *et al.*, "Microwave interrogated cascaded fiber Mach-Zehnder interferometer for optical length measurement," in *AOPC 2020: Optical Information and Network*, Beijing, 2020, pp. 1156907.

[69] Q. Chen, L. Gui, Y. Zhu, M. Wu, Q. Shen, and Y. Zhang, "Research on type sensing of optical fiber connector using microwave photonic interference," *Optics Frontiers Online 2020: Distributed Optical Fiber Sensing Technology and Applications. SPIE*, 2021, 11607: 89–93.

[70] X. Li, J. Liu, Z. Zou, and L. Zhan, "Tunable microwave photonic filters based on double-sideband modulation and linear chirped fibre Bragg gratings," *Journal of Modern Optics*, 2021, 68(12): 641–646.

[71] A. Ricchiuti, D. Barrera, S. Sales, L. Thevenaz, and J. Capmany, "Long fiber Bragg grating sensor interrogation using discrete-time microwave photonic filtering techniques," *Optics Express*, 2013, 21(23): 28175–28181.

[72] X. Zou, W. Pan, B. Luo, and L. Yan, "Full-scale phase demodulation approach for photonic instantaneous frequency measurement," *Optics Letters*, 2010, 35(16): 2747–2749.

[73] B. Cheng, L. Hua, Q. Zhang, J. Lei, and H. Xiao, "Microwave-assisted frequency domain measurement of fiber-loop ring-down system," *Optics Letters*, 2017, 42(7): 1209–1212.

[74] Z. Wang, S. Li, N. Wu, D. Zheng, and L. Xia, "Microwave-photonic interferometer based on FLRD for simultaneous sensing of loss and temperature," *Optics Communications*, 2023, 527(1): 128955.

[75] H. Chi, X. Zou, and J. Yao, "An approach to the measurement of microwave frequency based on optical power monitoring," *IEEE Photonics*

Technology Letters, 2008, 20(14): 1249–1251.

[76] W. Liu, H. Fu, P. Zhang, and S. He, "Fiber Bragg grating based wireless sensor module with modulated radio-frequency signal," *IEEE Microwave and Wireless Components Letters*, 2010, 20(6): 358–360.

[77] C. Zhu and J. Huang, "Sensitivity-enhanced microwave-photonic optical fiber interferometry based on the Vernier effect," *Optics Express*, 2021, 29(11): 16820–16832.

[78] L. Hua, X. Zhu, S. Dewolf, J. Lei, and H. Xiao, "Phase demodulation by frequency chirping in coherence microwave photonic interferometry," *IEEE Journal of Selected Topics in Quantum Electronics*, 2021, 27(99): 7700109.

[79] J. Huang, X. Lan, W. Zhu, B. Cheng, J. Fan, Z. Zhou, *et al.*, "Interferogram reconstruction of cascaded coaxial cable Fabry-Perot interferometers for distributed sensing application," *IEEE Sensors Journal*, 2016, 16(11): 4495–4450.

[80] M. Zhao, Y. Mao, Z. Wang, F. Yin, K. Xu, and Y. Dai, "Interferometric fiber-optic hydrophone system based on linear frequency modulation," *Journal of Lightwave Technology*, 2022, 40(20): 6769–6777.